analytical chemistry

pubs.acs.org/ac Article

A Three-Dimensional Electrochemical Biosensor Integrated with Hydrogel Enables Real-Time Monitoring of Cells under Their *In Vivo*-like Microenvironment

Xue-Bo Hu, Yu Qin, Wen-Ting Fan, Yan-Ling Liu,* and Wei-Hua Huang

Cite This: *Anal. Chem.* 2021, 93, 7917−7924 Read Online

ACCESS | Metrics & More | Article Recommendations | Supporting Information

ABSTRACT: Three-dimensional (3D) cell culture can better reproduce the *in vivo* cell environment and has been extensively used in fields such as tissue engineering, drug screening, and pathological research. Despite the tremendous advancement of 3D cultures, an analysis technique that could collect real-time information of the biological processes therein is sorely lacking. Electrochemical sensing with fast response and high sensitivity has played a vital role in real-time monitoring of living cells, but most current sensors are based on planar electrodes and fail to perfectly match the 3D cell culture matrix. Herein, we developed a robust 3D electrochemical sensor based on functionalized graphene foam (GF), which could be integrated with hydrogels for the 3D culture and *in situ* monitoring of cells for the first time. Specifically, platinum nanoparticles (Pt NPs) electrodeposited on GF (GF/Pt NPs) conferred the prominent electrochemical sensing performance, and the anti-fouling coating of poly(3,4-ethylenedioxythiophene) (PEDOT) endowed the GF/Pt NPs electrode with greatly improved stability. As a proof of concept, collagen hydrogel with microglia seeded in was filled into the interspace of the 3D GF/Pt NPs/PEDOT sensor to establish an integrated platform, which allowed the successful real-time monitoring of reactive oxygen species released from microglia in the collagen matrix. Given the versatility, our proposed biosensor in conjunction with various 3D culture models will serve as an excellent tool to provide biochemical information of cells under their *in vivo*-like microenvironment.

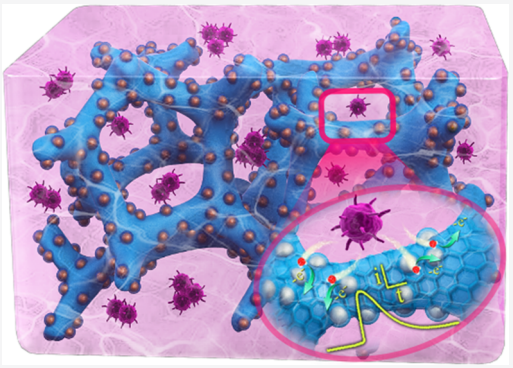

Three-dimensional (3D) cell culture has become a powerful platform for investigating the cell behavior and function in development, physiology, and pathophysiology owing to the distinct advantage on reproducing more analogous and predictive *in vivo* biological events over a traditional two-dimensional (2D) culture.[1−3] In the past decades, great advances have been made on functionalized materials (e.g., polymer scaffolds and naturally derived or synthetic hydrogels) and cell culture models derived from microfluidic technology to mimic the architecture of native cellular microenvironments.[4−6] With established 3D cell culture systems, what is rightly needed is the techniques for evaluating the behavior and function of cells cultured therein. Confocal fluorescence microscopy based on fluorescent staining is commonly performed to *in situ* quantify the cell number, morphology, and viability,[7,8] and analysis techniques like western blotting and enzyme-linked immunosorbent assays are often adopted to characterize specific biomarkers in cell lysis solution or a culture medium.[7,9] However, these endpoint analyses normally need to sacrifice the cultured cells or take some time for sampling, thus hampering the acquisition on the dynamic biological information.

Electrochemistry has been a powerful tool for the real-time monitoring of biological systems both *in vitro* and *in vivo* owing to the high sensitivity and fast response as well as the nondestructive and label-free measurement.[10−16] In this view, the combination of electrochemical sensing with the 3D cell culture system should be an artful design to achieve real-time monitoring of biochemical responses in 3D cultures. Actually, some attempts have been made by culturing cells in collagen and amino acid-based and dipeptide-derived hydrogels,[17−21] which were subsequently dispensed on the surface of planar electrodes (e.g., indium tin oxide and glass carbon), and therefore, the biomolecules released from cells in these 3D hydrogels could be detected by the underlying electrochemical sensors. Nonetheless, these experimental configurations were not fully satisfactory. Because the molecules released from cells diffuse in all directions, only those which spread to the surface of underlying planar sensors could be detected.[19] Meanwhile, the long diffusion distance between the cells in the 3D matrix and the electrode may lead to an unreliable result since

Received: February 9, 2021
Accepted: May 12, 2021
Published: May 21, 2021

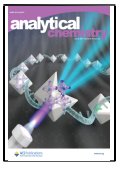

https://doi.org/10.1021/acs.analchem.1c00621
Anal. Chem. 2021, 93, 7917−7924

Scheme 1. Schematic Illustration of the Fabrication Processes of the 3D GF/Pt NPs/PEDOT Electrochemical Sensor and Collagen Hydrogel Integrated Platform

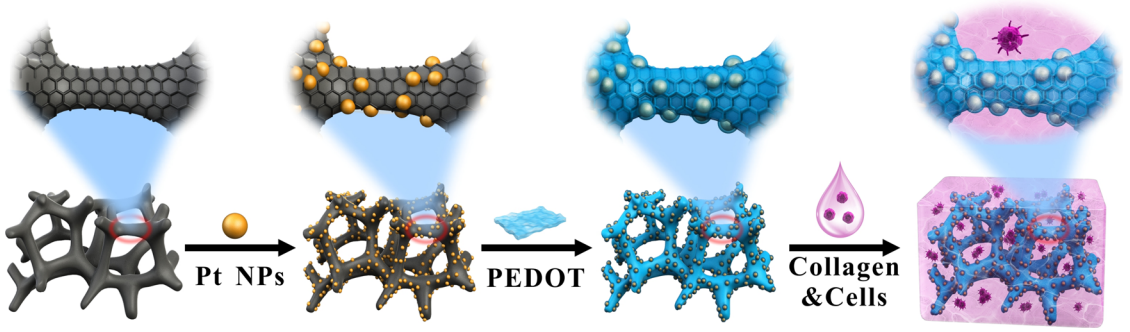

molecules with a very short half-life (e.g., $O_2^{\cdot-}$ and NO)[11] will disappear in the diffusion process. To solve this problem, embedding a 3D electrochemical sensor into a 3D cell culture matrix will be convincingly an effective strategy.

Although few 3D electrochemical sensors based on graphene foam (GF) and a conductive polymer have been reported,[22−26] they have not yet been integrated with the 3D matrix for cell culture and detection. Considering that electrochemical sensors will be surrounded by complex environments, two critical factors should be carefully concerned for the successful fabrication of a 3D integrated platform. On one hand, since the released molecules must cross the 3D matrix before the arrival on the fixed electrode, high sensitivity of the implanted sensor is the precondition to achieve real-time monitoring of cells.[19,23,24] On the other hand, the 3D sensor will be exposed to complex cell culture environments, which would easily lead to the biofouling of the sensing interface by the culture medium or cell-released biomolecules,[27−29] and thus maintaining the stability of the implanted 3D sensor is another key point.

Motivated by these issues, in this work, we reported a robust 3D electrochemical sensor based on a functionalized graphene scaffold, which was embedded in collagen hydrogel for modeling the extracellular matrix and real-time monitoring of cells cultured therein. With regard to the fabrication, Pt nanoparticles (NPs) were electrodeposited on the surface of 3D GF (GF/Pt NPs) to improve sensitivity. Then, a PEDOT ultrathin film was introduced to retard the biofouling in a complex environment. As a proof of concept, collagen hydrogel with microglial cells encapsulated therein was filled in the interspace of the as-prepared 3D GF/Pt NPs/PEDOT electrochemical sensor and finally formed a 3D biohybrid system (Scheme 1). This integrated platform allowed *in situ* and real-time monitoring of reactive oxygen species (ROS) from microglial cells cultured in a 3D matrix. This work provides an effective, real-time detection platform for 3D cell culture systems and is expected to facilitate various physiological and pathological relevant researches.

EXPERIMENTAL SECTION

Materials and Instruments. Nickel foam (1.65 mm in thickness; porosity ≥95%) was bought from Alantum Advanced Technology Materials (China). Collagen solution (rat tail collagen type I, 3.5 mg/mL) was purchased from Corning (U.S.A.). Lipopolysaccharides (LPS, from *Escherichia coli* O55:B5), interferon γ (IFN-γ), diphenyleneiodonium chloride ($C_{12}H_8ClI$, DPI), 3,4-ethoxylenedioxythiophene ($C_6H_6O_2S$, EDOT), and a Calcein-AM/PI (live/dead cell) double staining kit were purchased from Sigma-Aldrich (U.S.A.). BV2 cells were obtained from the China Center for Type Culture Collection (China). The cell culture medium and related supplements were bought from Gibco Corp. (Grand Island, NY). Chloroplatinic acid hexahydrate ($H_2PtCl_6{\cdot}6H_2O$) was obtained from the Reagent No.1 Factory of Shanghai Chemical Reagent Co., Ltd. (China). Other chemicals were reagent grade and used as obtained without further purification. For all the experiments, ultrapure water (Millipore, 18.2 MΩ) was used.

Scanning electron microscopy (SEM) images were obtained by using a field-emission microscope (Zeiss Sigma), and energy-dispersive X-ray spectroscopy (EDX) for elemental mapping images was acquired by using an INCAPentalFETx3 Oxford EDX spectrometer. Transmission electron microscopy (TEM) images were obtained on a JEM-2100 at an acceleration voltage of 200 kV. Raman spectroscopy was performed with a laser micro-Raman spectrometer (Renishaw, 532 nm excitation wavelength). X-ray photoelectron spectroscopy (XPS) measurements were conducted on an ESCALAB 250Xi photoelectron spectrometer (Thermo Fisher Scientific, Al Kα X-ray radiation). X-ray diffraction (XRD) measurements were performed by a LabX XRD-6000 (Cu Kα radiation) over the range of $2\theta = 20-90°$. Inverted fluorescence microscopes (AxioObserver Z1 and Axiovert 200 M, Zeiss) and a laser scanning confocal microscope (PerkinElmer, UltraView Vox System) were used for the observation of cells and fluorescence imaging. All the electrochemical measurements were conducted on a CHI 660A electrochemical workstation (CHI Instruments) at room temperature.

Fabrication of the GF/Pt NPs/PEDOT Electrode. The chemical vapor deposition process of GF on nickel foam was based on a previously developed method.[30] After nickel was removed, Pt NPs were electrodeposited on the GF by cyclic voltammetry (CV) scanning in the electrolyte at a potential of −0.5 to +0.3 V (vs Ag/AgCl) for different times, which contained 0.2 M Na_2SO_4 and 30 mM H_2PtCl_6. To obtain the PEDOT-coated GF/Pt NPs electrode, the GF/Pt NPs electrode was immersed into an electrolyte containing 10 mM EDOT and 2 mg/mL PSS. Under a constant potential of +1.0 V for different time, PEDOT was deposited on the GF/Pt NPs electrode.[31]

3D Cell Culture and Real-Time Monitoring. BV2 cells were cultured in Dulbecco's modified Eagle's medium (DMEM) with 1% penicillin−streptomycin and 10% fetal bovine serum in a cell culture incubator (37 °C and 5% CO_2, HERACELL 150i, Thermo Fisher Scientific). To culture BV2 cells in the 3D matrix, collagen was mixed with DMEM and

https://doi.org/10.1021/acs.analchem.1c00621
Anal. Chem. 2021, 93, 7917−7924

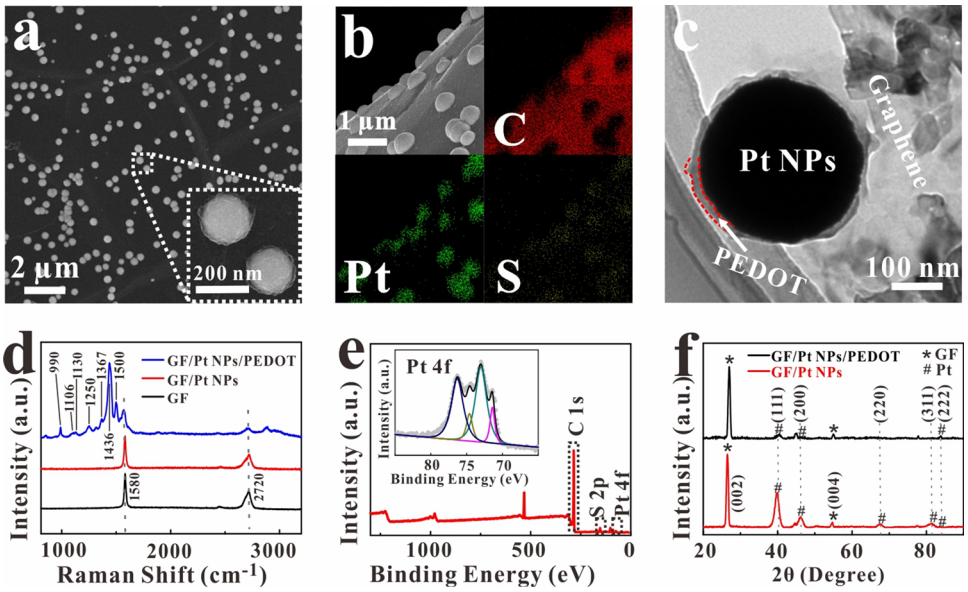

Figure 1. (a) SEM images of the surface of GF/Pt NPs/PEDOT composites and the inset shows the enlarged SEM image of the area in the white dashed rectangle. (b) High-magnification SEM image of GF/Pt NPs/PEDOT and the corresponding EDX elemental mapping images of C (red), Pt (green), and S (yellow). (c) TEM image of GF/Pt NPs/PEDOT, in which the area between the two red dashed lines represents the PEDOT film. (d) Raman spectra of GF/Pt NPs/PEDOT (blue line), GF/Pt NPs (red line), and GF (black line). (e) XPS spectrum of the GF/Pt NPs/PEDOT composites and the inset shows the Pt 4f states. (f) XRD patterns of GF/Pt NPs/PEDOT (black line) and GF/Pt NPs (red line).

the pH was adjusted to about 7.2 at 4 °C. Then, the above cell loading solution was quickly perfused into the GF/Pt NPs/PEDOT electrode to form the collagen-incorporated GF/Pt NPs/PEDOT platform. For SEM characterization, BV2 cells with a density of ~1×10^5 cell/mL were seeded into the above composites and culture medium-mixed solution at 4 °C. For cell-related electrochemical experiments, BV2 cells with a density of ~1×10^6 cell/mL were seeded into collagen. To measure the ROS released from the BV2 cells, the amperometric responses of GF/Pt NPs/PEDOT were recorded with cells stimulated with 10 mM LPS and 5 mM IFN-γ (LPS/IFN-γ). In control experiments, BV2 cells were treated without LPS/IFN-γ or pre-incubated with DPI (NADPH oxidase inhibitor) before the LPS/IFN-γ stimulation.

RESULTS AND DISCUSSION

Preparation and Characterization of the 3D GF/Pt NPs/PEDOT Electrode. First, 3D GF was obtained via chemical vapor deposition, as previously reported.[30] High-quality synthesis endows GF with superior conductivity,[32] while its electrochemical activity is relatively low due to the lack of defect sites (Figure S1a). To improve the electrochemical performance, Pt NPs, widely accepted electrocatalysts, were deposited on the surface of the GF scaffold. As shown in Figure S1, the amount of Pt NPs deposited on GF could be precisely controlled by the electrodeposition process. With cyclic voltammetry proceeding (0, 6, 12, and 24 cycles), the amount of Pt NPs on the GF obviously increased, and the peak currents of cyclic voltammograms recorded on the corresponding GF/Pt NPs electrodes in 1 mM $K_3[Fe(CN)_6]$ also gradually increased (Figure S1). It should be noted that, although the electrode obtained by 24 cycles showed the biggest peak current, the Pt NPs seriously aggregated with each other and even exfoliated from the surface of the GF scaffold (Figure S1d). Considering the balance between electrochemical sensing and stability, the GF/Pt NPs electrode with the electrodeposition of Pt NPs for 12 cycles was adopted in the following experiments. The TEM image in Figure S2 demonstrates that the Pt NPs with an average diameter of *ca.* 200 nm were tightly anchored on the surface of graphene, and the corresponding high-resolution TEM image (Figure S2b) exhibited the (111) plane of Pt (lattice fringes with a *d* spacing of 0.226 nm).[33]

PEDOT is a widely used electrode material with a good electrochemical property and stability, and recently increasing reports have revealed its anti-fouling performance.[29,34,35] The electropolymerization method was employed to coat the surface of the GF/Pt NPs electrode with PEDOT in a controlled way by adjusting the reaction time.[31] As illustrated in Figure S3, the surface of the GF/Pt NPs electrode became rougher as the electropolymerization proceeded, indicating that the PEDOT film on the GF/Pt electrode gradually thickened. Regarding the characterization, the GF/Pt NPs/PEDOT electrode with PEDOT electropolymerized for 20 s was taken as an example to analyze the morphology and elements. The SEM image showed that uniform Pt NPs were deposited on the surface of the GF electrode, and the enlarged image showed that Pt NPs were encapsulated by thin films (Figure 1a). The high-resolution SEM image and EDX mapping displayed the distribution of C (red), Pt (green), and S (yellow) elements, which corresponded to GF, Pt NPs, and PEDOT, respectively (Figure 1b). The TEM image illustrated that the thickness of the PEDOT film covered on the surface of GF/Pt NPs was about 15 nm (Figure 1c).

Raman spectra were conducted to confirm the layer and the quality of GF/Pt NPs/PEDOT. As shown in Figure 2d, two peaks centered at 1580 cm^{-1} (G band) and 2720 cm^{-1} (2D band) can be found in all the spectra of GF, GF/Pt NPs, and GF/Pt NPs/PEDOT, and the intensities of these two bands indicated the multilayer property of graphene.[32] After the functionalization of Pt NPs and PEDOT on GF, several new peaks in the range of 990−1500 cm^{-1} that corresponded to the

https://doi.org/10.1021/acs.analchem.1c00621
Anal. Chem. 2021, 93, 7917−7924

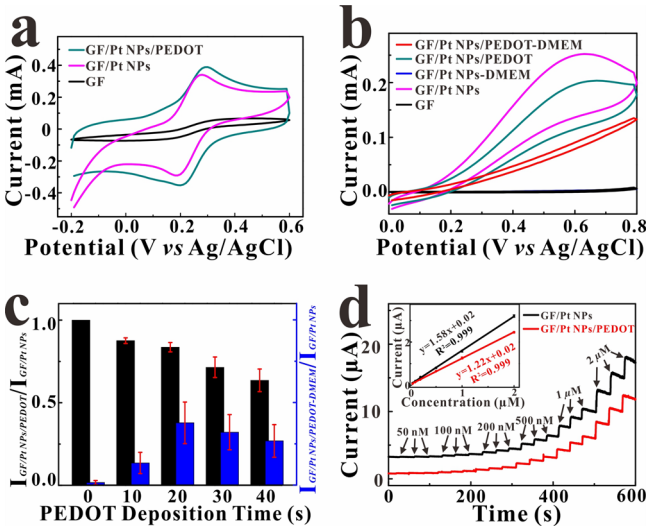

Figure 2. CV curves of different electrodes obtained in (a) 1 mM $K_3[Fe(CN)_6]$ and (b) PBS containing 1 mM H_2O_2. (c) Statistical results of the oxidation peak current in H_2O_2 solution of GF/Pt NPs electrodes after and before PEDOT deposition ($I_{GF/Pt\ NPs/PEDOT}/I_{GF/Pt\ NPs}$, black column) and the GF/Pt NPs/PEDOT electrode after being fouled by the DMEM electrode to the original GF/Pt NPs electrode ($I_{GF/Pt\ NPs/PEDOT\text{-}DMEM}/I_{GF/Pt\ NPs}$, blue column). (d) Amperometric responses of GF/Pt NPs/PEDOT (red line) and GF/Pt NPs (black line) electrodes to a series of H_2O_2 concentration increases in a stirred PBS solution at a potential of +0.60 V (vs Ag/AgCl). The inset represents the corresponding calibration curves.

specific bands of PEDOT and PSS appeared,[36−38] but no peaks centered at the disorder-induced D band (1350 cm^{-1}) were found, demonstrating that almost no defects were introduced to the original high-quality graphene during the electrodeposition and electropolymerization processes.

XPS and XRD characterizations were conducted to further analyze the existing form of individual elements. The peaks of C, S, and Pt could be found in the wide survey XPS spectrum of GF/Pt NPs/PEDOT (Figure 1e), and the spectrum of the Pt 4f state consisted of four peaks centered at 71.4, 74.4, 73.0, and 76.3 eV (Figure 1e, inset), corresponding to the $4f_{7/2}$ and $4f_{5/2}$ peaks of Pt(0) and Pt(II), respectively.[39−41] In addition, the deconvolution of C 1s and S 2p spectra is also analyzed in Figure S4. XRD characterization showed that two peaks centered at about 26.4 and 54.5° could be found in both GF/Pt NPs and GF/Pt NPs/PEDOT composites (Figure 2f), which were attributed to the (002) and (004) reflections of graphitic carbon (JCPDS card 75-1621), respectively.[42] Another four peaks of GF/Pt NPs composites centered at about 40.0, 46.2, 67.5, and 81.3° belonged to the (111), (200), (220), and (311) reflections of Pt NPs (JCPDS card 65-2868), respectively.[43,44] After the deposition of PEDOT, the intensity of Pt NPs dramatically dropped due to the encapsulation of PEDOT. Together, all these results confirmed that the Pt NPs and PEDOT had been successfully decorated on the surface of the 3D GF scaffold.

Electrochemical Performance of the GF/Pt NPs/PEDOT Electrode. The electrochemical responses of GF, GF/Pt NPs, and GF/Pt NPs/PEDOT electrodes toward $[Fe(CN)_6]^{3-/4-}$ were characterized (Figure 2a). Compared with the GF electrode with pure graphene, the GF/Pt NPs electrode exhibited much larger peak currents, and this clearly indicated that Pt NPs as an excellent catalyst could significantly increase the electrode-active area and facilitate electron transfer between the electrode and $[Fe(CN)_6]^{3-/4-}$. Importantly, the subsequent deposition of the outer PEDOT thin film had a negligible influence on the performance of the GF/Pt NPs electrode.

To evaluate the electrochemical sensing property, hydrogen peroxide (H_2O_2) was selected as the target molecule due to its critical role in regulating diverse biological processes.[45,46] As shown in Figure 2b, the peak current of the GF/Pt NPs electrode was almost 30 times higher than that of the GF electrode, demonstrating the excellent electrocatalytic activity of Pt NPs toward H_2O_2 electrooxidation. After the electropolymerization of PEDOT, the peak current (at +0.60 V) could still maintain about 80% that of the GF/Pt NPs electrode. Regarding the retained satisfying performance, it was due to the fact that the electrodeposited PEDOT films usually possess a porous structure,[47,48] and thus the small molecules like H_2O_2 could permeate across the thin PEDOT layer (about 15 nm) to the active sites of Pt nanoparticles. When GF/Pt NPs and GF/Pt NPs/PEDOT electrodes were immersed in the DMEM medium for 1 day to preliminarily mimic cell environments, no obvious oxidation peak could be recorded on the GF/Pt NPs electrode in H_2O_2 solution (the CV curve coincides with that of GF), while the current of the GF/Pt NPs/PEDOT electrode remained about 55% of the original unfouled electrodes and about 28 times of the fouled GF/Pt NPs electrode. In addition, the GF/Pt NPs/PEDOT electrode was further treated with more complex biosystems, that is, collagen and the DMEM system with or without cells cultured therein, and the current of fouled electrodes also remained 40 and 49% of the original unfouled electrode (Figure S5). The above results convincingly proved that the existence of the PEDOT film greatly improved the electrochemical stability of the GF/Pt NPs/PEDOT electrode.

Since it was Pt NPs rather than PEDOT that contributed electrochemical activity to the H_2O_2 electrooxidation (Figure S6), the amount of PEDOT deposited on GF/Pt NPs should be precisely controlled to achieve the good balance between electrochemical sensing and anti-fouling performance. Therefore, the GF/Pt NPs/PEDOT electrodes with PEDOT deposited for different times (0, 10, 20, 30, and 40 s) were fabricated, and the peak currents of these electrodes obtained in the same H_2O_2 solution before or after DMEM treatment were compared with the original GF/Pt NPs electrodes (Figure 2c). The results illustrated that, with the increase in deposition time, the ratio of the peak current of the GF/Pt NPs/PEDOT electrode ($I_{GF/Pt\ NPs/PEDOT}$) to the GF/Pt NPs electrode ($I_{GF/Pt\ NPs}$) gradually decreased, demonstrating that excessive PEDOT would block the active sites on the surface of Pt NPs. After being immersed in the DMEM medium for 1 day, the ratio of the peak current of the GF/Pt NPs/PEDOT electrode ($I_{GF/Pt\ NPs/PEDOT\text{-}DMEM}$) to the original GF/Pt NPs electrode ($I_{GF/Pt\ NPs}$) gradually increased and reached the maximum with PEDOT deposited for 20 s.

To further investigate the effect of PEDOT coating on electrochemical sensing performance, the same GF/Pt NPs electrode before and after the deposition of PEDOT for 20 s was employed for the amperometric detection of different concentrations of H_2O_2. As displayed in Figure 2d, the corresponding calibration curves of GF/Pt NPs and GF/Pt NPs/PEDOT electrodes demonstrated good linear relation in the range of 50 nM to 2 μM, and the sensitivities of the two electrodes were calculated to be 1.58 and 1.22 μA/μM,

https://doi.org/10.1021/acs.analchem.1c00621
Anal. Chem. 2021, 93, 7917−7924

respectively. The results confirmed that PEDOT deposition on GF/Pt NPs for 20 s still maintained 77% of the original sensitivity, which is in accordance with the result displayed in Figure 2c. The detection limits (S/N = 3) of the GF/Pt NPs and GF/Pt NPs/PEDOT electrodes toward H_2O_2 detection were calculated to be 10 and 17 nM, respectively.

3D Cell Culture in the GF/Pt NPs/PEDOT and Collagen Integrated Platform. Naturally derived polymers, such as collagen and fibrin, are important extracellular matrixes in the 3D cell culture to construct a cell microenvironment due to the inherent biocompatibility and bioactivity.[6,49,50] Here, collagen type I was selected to be the material for the 3D cell culture in the platform. The cell culture state was investigated by culturing BV2 cells in a culture dish and collagen for 3 days and staining with fluorescent live/dead cell markers Calcein-AM and PI. The fluorescence microscopic images shown in Figure 3a,b demonstrate that both of the cells cultured in collagen or a culture dish were in high viability. Notably, the cells in the 2D culture dish were characterized with the spindle shape as individuals (Figure 3a), while cells cultured inside collagen displayed the spherical shapes and resided in the agglomeration state (Figure 3b). This morphological distinction reflected the superiority of the 3D cell culture in reproducing the *in vivo* cell behavior and function.

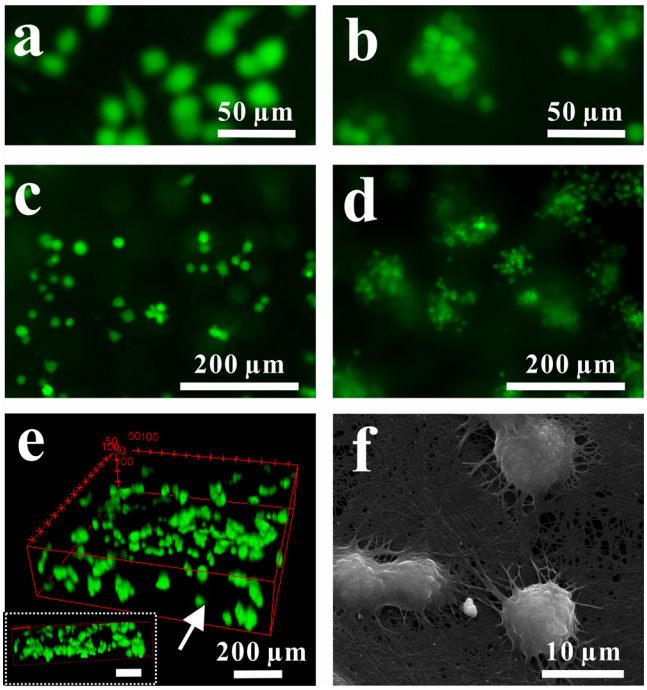

Figure 3. Merged fluorescence microscopic images of BV2 cells stained with Calcein-AM (green) and PI (red) after being cultured in a (a) cell culture dish, (b) collagen matrix for 3 days, and collagen and 3D GF/Pt NPs/PEDOT electrode integrated platform for (c) 4 h and (d) 84 h. (e) 3D reconstruction of constructs from LSCM images of BV2 cells cultured in the integrated platform for 1 day and stained with Calcein-AM and PI. The inset displays the sectional view in the direction of the white arrow, and the scale bars are 200 μm. (f) SEM image of BV2 cells cultured in the integrated platform for 1 day.

To investigate the proliferation of cells cultured in a 3D integrated platform, the collagen solution containing dispersed BV2 cells was perfused into the 3D GF/Pt NPs/PEDOT electrode. At the beginning, individual BV2 cells were dispersed in the 3D interspace of the electrode (Figure 3c). After the cells were cultured for 84 h, numerous cell clusters were observed in different areas of the platform (Figure 3d), indicating the good proliferation ability of BV2 cells cultured therein, and the laser scanning confocal microscopy (LSCM) result further revealed that the cell clusters distributed all around the interspace of collagen at different heights (Figure 3e). SEM characterization demonstrated that the porous structure of GF/Pt NPs/PEDOT was filled with the collagen fibers (Figure 3f and Figure S7), BV2 cells distributed on the skeletons of the GF/Pt NPs/PEDOT scaffold or inside the collagen, and some of the cells are partly or fully encapsulated by collagen. Taken together, cells cultured in the collagen and 3D GF/Pt NPs/PEDOT electrode integrated platform kept high viability and good proliferation ability.

Real-Time Monitoring of ROS Release from Cells in the 3D Culture and Detection Platform. With the satisfying performance of sensitivity and stability, the real-time and *in situ* monitoring of ROS released from BV2 cells could be investigated (Figure 4a). Before the electrochemical detection, fluorescence staining by DCFH-DA (a peroxide/redox-sensitive fluorescent probe) was performed to confirm that the LPS/IFN-γ (as pro-inflammatory factor[51]) stimulation could evoke the production of ROS in BV2 cells (Figure 4b). It was obviously identified that the level of ROS in cells after stimulation (15 and 30 min) was much higher than that of cells without stimulation, and the results of endpoint analysis showed that the intracellular ROS appeared to accumulate with the inflammation proceeding. The shapes of BV2 cells changed from a ramified state to an amoeboid morphology, which is in accordance with the physiological process of activated microglia.[51] In addition, the immunostaining of the microglial protein marker OX42[52] also confirmed that the BV2 cells in the experiments maintained the morphology and function of the primary microglia (Figure S8).

Subsequently, after BV2 cells were cultured in the 3D integrated platform for 12 h, the cells were stimulated by LPS/IFN-γ to induce inflammation and ensuing ROS release. As shown in Figure 4c, there were many spikes on the amperometric curve recorded by the embedded GF/Pt NPs/PEDOT electrode (Figure 4d, red line). These independent spikes, unlike a previously reported signal featured by a continuous increase and slow decrease in current,[24,26] might result from the unique 3D biohybrid cell culture and monitoring system. On one hand, the LPS/IFN-γ stimulation generally evokes inflammatory response with asynchronous and long-term ROS bursts from large amounts of BV2 cells (as shown in Figure 4b).[51] On the other hand, the ROS released from BV2 cells in collagen hydrogel need different times to diffuse to the surface of the 3D sensor. To confirm that the current spikes were caused by ROS bursts from activated BV2 cells in response to the LPS/IFN-γ stimulation, the 3D integrated platform without cells cultured inside was also stimulated under the same conditions and no spikes were found in the current curve (Figure 4c, black line). When BV2 cells were pre-incubated by DPI for 30 min and further stimulated by LPS/IFN-γ, only a few spikes with low currents were observed (Figure 4c, blue line). This could be attributed to the inhibition of DPI on the activity of NADPH oxidase, which is the predominant enzyme of the microglia to produce ROS.[53] Notably, after being stimulated by LPS/IFN-γ and electrochemically monitored long for 4 h, nearly all the BV2 cells far from or near the GF/Pt NPs/PEDOT electrode kept a

https://doi.org/10.1021/acs.analchem.1c00621
Anal. Chem. 2021, 93, 7917−7924

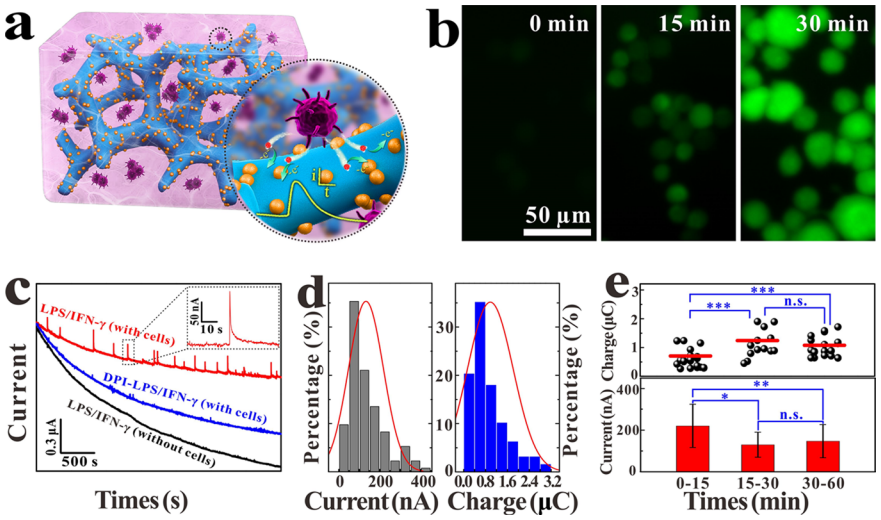

Figure 4. (a) Schematic illustration of real-time and *in situ* monitoring of ROS released from BV2 cells cultured in the integrated platform. (b) Fluorescence microphotographs of BV2 cells stained with DCFH-DA without (0 min) or with the incubation of LPS/IFN-γ for different times: 15 and 30 min. (c) Amperometric response of the 3D biosensor under different conditions. (d) Current responses and the charge of the spikes recorded from six different electrodes (130 spikes) after BV2 cells were cultured for 12 h and stimulated with LPS/IFN-γ (left side: current; right side: charge). (e) Statistical results of ROS release detected from BV2 cells for different periods after the LPS/IFN-γ stimulation (downside: current; upside: charge. $^{*}P < 0.05$, $^{**}P < 0.01$, and $^{***}P < 0.001$).

high viability as evidenced by the fluorescent live/dead cell markers Calcein-AM and PI (Figure S9), indicating that the activated BV2 cells still retained their normal functions.

Next, to acquire the quantitative information about the ROS released from activated BV2 cells, the current and charge (time integral of current) of 130 spikes collected from the current curves of six measurements were counted (Figure 4d). The average value of current spikes was calculated to be 130 nA (Figure 4d, left), and the corresponding concentration of ROS was about 90 nM according to the calibration curve. The average charge of the spikes was calculated to be 990 nC (Figure 4d, right). Further considering that the ROS bursts from BV2 cells during different stages of inflammation may differ from each other, the current responses of three time periods (0−15, 15−30, and 30−60 min) after the LPS/IFN-γ stimulation were analyzed (Figure 4e, down), and the average currents were 220, 130, and 147 nA, respectively. Furthermore, the charge of the three different time periods was also analyzed and the average charges were calculated to be 600, 1090, and 987 nC (Figure 4e, top), respectively. The results revealed that the concentrations of ROS released in different time periods were different from each other, which exactly represents the great advantage of electrochemical sensing on the real-time and *in situ* monitoring of cells, compared with endpoint analysis methods. In addition, further quantitative analysis could be conducted by modeling the sensor response with specific parameters (e.g., cell distribution, the diffusion rate of secreted biomolecules, and the viscosity of matrix), which is expected to promote the research based on the 3D cell culture, such as signaling molecule gradients in immunology[54] and 3D tumor microenvironments.[55]

CONCLUSIONS

In summary, we for the first time developed a robust 3D biohybrid platform by embedding a 3D electrochemical sensor into collagen hydrogel for modeling the extracellular matrix and real-time monitoring of cells under their *in vivo*-like microenvironment. Pt NPs immobilization and the PEDOT coating endowed the sensor with high sensitivity and satisfying anti-fouling performance, respectively. These ensured the excellent sensing stability of the sensor when interfacing with and embedding into hydrogel. As a proof of concept, the ROS released from activated microglia cultured in collagen was successfully monitored in real time by the embedded 3D electrochemical sensor, representing an important step toward the acquisition of dynamic biochemical information in the 3D cell culture. Considering that the GF/Pt NPs/PEDOT electrode could be further endowed with more functionalities (e.g., a high-efficiency catalyst and specific recognition system to improve the sensitivity and selectivity), our present electrochemical device as an efficient tool is expected to promote many 3D cell culture-related biomedical researches, such as cell metastasis, tissue engineering, immunotherapy, drug discovery, and screening.

ASSOCIATED CONTENT

Supporting Information

The Supporting Information is available free of charge at https://pubs.acs.org/doi/10.1021/acs.analchem.1c00621.

SEM images and electrochemical performance of GF and GF/Pt NPs with different cycling times, TEM images of GF/Pt NPs, SEM images GF/Pt NPs and GF/Pt NPs/PEDOT with different PEDOT deposition times, XPS spectra of the C 1s and S 2p state in GF/Pt NPs/PEDOT composites, CV curves of GF/Pt NPs/PEDOT before or after being treated by collagen and DMEM cultured with or without cells toward PBS and H_2O_2, CV curves of GF/PEDOT toward PBS and H_2O_2, SEM images of cells cultured in the 3D integrated platform, and optical and fluorescence microphotographs of BV2 cells stained with OX42 and BV2 cells stained with Calcein-AM/PI after electrochemically monitored for 4 h (PDF)

https://doi.org/10.1021/acs.analchem.1c00621
Anal. Chem. 2021, 93, 7917−7924

AUTHOR INFORMATION

Corresponding Author

Yan-Ling Liu − *College of Chemistry and Molecular Sciences, Wuhan University, Wuhan 430072, China;* orcid.org/0000-0002-7386-354X; Email: yanlingliu@whu.edu.cn

Authors

Xue-Bo Hu − *College of Chemistry and Molecular Sciences, Wuhan University, Wuhan 430072, China; College of Chemistry and Chemical Engineering, Institute for Conservation and Utilization of Agro-bioresources in Dabie Mountains, Xinyang Normal University, Xinyang 464000, China*

Yu Qin − *College of Chemistry and Molecular Sciences, Wuhan University, Wuhan 430072, China*

Wen-Ting Fan − *College of Chemistry and Molecular Sciences, Wuhan University, Wuhan 430072, China*

Complete contact information is available at: https://pubs.acs.org/10.1021/acs.analchem.1c00621

Author Contributions

The manuscript was written through contributions of all authors. All authors have given approval to the final version of the manuscript.

Notes

The authors declare no competing financial interest.

ACKNOWLEDGMENTS

This work was supported by the National Natural Science Foundation of China (grants 21725504, 21804101, 22090051, and 21721005).

REFERENCES

(1) Khawar, I. A.; Park, J. K.; Jung, E. S.; Lee, M. A.; Chang, S.; Kuh, H. J. *Neoplasia* **2018**, *20*, 800−812.
(2) Cho, H. J.; Verbridge, S. S.; Davalos, R. V.; Lee, Y. W. *Ann. Biomed. Eng.* **2018**, *46*, 877−887.
(3) Lovett, M. L.; Nieland, T. J.; Dingle, Y. T. L.; Kaplan, D. L. *Adv. Funct. Mater.* **2020**, *30*, 1909146.
(4) Edmondson, R.; Broglie, J. J.; Adcock, A. F.; Yang, L. *Assay Drug. Dev. Technol.* **2014**, *12*, 207−218.
(5) Page, H.; Flood, P.; Reynaud, E. G. *Cell Tissue Res.* **2013**, *352*, 123−131.
(6) Huang, G.; Li, F.; Zhao, X.; Ma, Y.; Li, Y.; Lin, M.; Jin, G.; Lu, T. J.; Genin, G. M.; Xu, F. *Chem. Rev.* **2017**, *117*, 12764−12850.
(7) Castiaux, A. D.; Spence, D. M.; Martin, R. S. *Anal. Methods* **2019**, *11*, 4220−4232.
(8) Frey, O.; Misun, P. M.; Fluri, D. A.; Hengstler, J. G.; Hierlemann, A. *Nat. Commun.* **2014**, *5*, 4250.
(9) Yu, Y. J.; Kim, Y. H.; Na, K.; Min, S. Y.; Hwang, O. K.; Park, D. K.; Kim, D. Y.; Choi, S. H.; Kamm, R. D.; Chung, S.; Kim, J. A. *Lab Chip* **2018**, *18*, 2604−2613.
(10) Paleček, E.; Dorčák, V. *Appl. Mater. Today* **2017**, *9*, 434−450.
(11) Amatore, C.; Arbault, S.; Guille, M.; Lemaitre, F. *Chem. Rev.* **2008**, *108*, 2585−2621.
(12) Zhang, M.; Yu, P.; Mao, L. *Acc. Chem. Res.* **2012**, *45*, 533−543.
(13) Phan, N. T. N.; Li, X.; Ewing, A. G. *Nat. Rev. Chem.* **2017**, *1*, 0048.
(14) Zhang, L.; Tian, Y. *Acc. Chem. Res.* **2018**, *51*, 688−696.
(15) Yu, R. J.; Ying, Y. L.; Gao, R.; Long, Y. T. *Angew. Chem., Int. Ed.* **2019**, *58*, 3706−3714.
(16) Liu, Y. L.; Huang, W. H. *Angew. Chem., Int. Ed.* **2021**, *60*, 2757−2767.
(17) Pan, L.; Yu, G.; Zhai, D.; Lee, H. R.; Zhao, W.; Liu, N.; Wang, H.; Tee, B. C.-K.; Shi, Y.; Cui, Y.; Bao, Z. *Proc. Natl. Acad. Sci. U. S. A.* **2012**, *109*, 9287−9292.
(18) Zhou, J.; Liao, C.; Zhang, L.; Wang, Q.; Tian, Y. *Anal. Chem.* **2014**, *86*, 4395−4401.
(19) Lian, M.; Xu, L.; Zhu, X.; Chen, X.; Yang, W.; Wang, T. *Anal. Chem.* **2017**, *89*, 12843−12849.
(20) Santos-Cancel, M.; Simpson, L. W.; Leach, J. B.; White, R. J. *ACS Chem. Neurosci.* **2019**, *10*, 2070−2079.
(21) Liu, M. M.; Guo, Z. Z.; Liu, H.; Li, S. H.; Chen, Y.; Zhong, Y.; Lei, Y.; Lin, X. H.; Liu, A. L. *Biosens. Bioelectron.* **2019**, *144*, 111686.
(22) Xi, F.; Zhao, D.; Wang, X.; Chen, P. *Electrochem. Commun.* **2013**, *26*, 81−84.
(23) Liu, J.; He, Z.; Xue, J.; Tan, T. T. Y. *J. Mater. Chem. B* **2014**, *2*, 2478−2482.
(24) Hu, X. B.; Liu, Y. L.; Wang, W. J.; Zhang, H. W.; Qin, Y.; Guo, S.; Zhang, X. W.; Fu, L.; Huang, W. H. *Anal. Chem.* **2018**, *90*, 1136−1141.
(25) Hu, F. X.; Guo, C.; Yang, H. B.; Shi, Z.; Wang, M.; Xue, Y. H.; Zhu, L.; Chen, T.; Dai, L.; Li, C. M. *Sens. Actuators, B* **2019**, *287*, 209−217.
(26) Zhang, H. W.; Hu, X. B.; Qin, Y.; Jin, Z. H.; Zhang, X. W.; Liu, Y. L.; Huang, W. H. *Anal. Chem.* **2019**, *91*, 4838−4844.
(27) Zhou, L.; Hou, H.; Wei, H.; Yao, L.; Sun, L.; Yu, P.; Su, B.; Mao, L. *Anal. Chem.* **2019**, *91*, 3645−3651.
(28) Liu, Y. L.; Chen, Y.; Fan, W. T.; Cao, P.; Yan, J.; Zhao, X. Z.; Dong, W. G.; Huang, W. H. *Angew. Chem., Int. Ed.* **2020**, *59*, 4075−4081.
(29) Jiang, C.; Wang, G.; Hein, R.; Liu, N.; Luo, X.; Davis, J. J. *Chem. Rev.* **2020**, *120*, 3852−3889.
(30) Hu, X.; Ma, M.; Zeng, M.; Sun, Y.; Chen, L.; Xue, Y.; Zhang, T.; Ai, X. P.; Mendes, R. G.; Rümmeli, M. H.; Fu, L. *ACS Appl. Mater. Interfaces* **2014**, *6*, 22527−22533.
(31) Hu, X. B.; Liu, Y. L.; Zhang, H. W.; Xiao, C.; Qin, Y.; Duo, H. H.; Xu, J. Q.; Guo, S.; Pang, D. W.; Huang, W. H. *ChemElectroChem* **2016**, *3*, 1998−2002.
(32) Chen, Z.; Ren, W.; Gao, L.; Liu, B.; Pei, S.; Cheng, H. M. *Nat. Mater.* **2011**, *10*, 424−428.
(33) Li, Y.; Tang, L.; Li, J. *Electrochem. Commun.* **2009**, *11*, 846−849.
(34) Xiao, X.; Wang, M.; Li, H.; Si, P. *Talanta* **2013**, *116*, 1054−1059.
(35) Yang, X.; Kirsch, J.; Olsen, E. V.; Fergus, J. W.; Simonian, A. L. *Sens. Actuators, B* **2013**, *177*, 659−667.
(36) Chiu, W. W.; Travaš-Sejdić, J.; Cooney, R. P.; Bowmaker, G. A. *J. Raman Spectrosc.* **2006**, *37*, 1354−1361.
(37) Schaarschmidt, A.; Farah, A. A.; Aby, A.; Helmy, A. S. *J. Phys. Chem. B.* **2009**, *113*, 9352−9355.
(38) Stavytska-Barba, M.; Kelley, A. M. *J. Phys. Chem. C* **2010**, *114*, 6822−6830.
(39) Parkinson, C. R.; Walker, M.; McConville, C. F. *Surf. Sci.* **2003**, *545*, 19−33.
(40) Maldonado-Hódar, F. J.; Moreno-Castilla, C.; Pérez-Cadenas, A. F. *Appl. Catal., B* **2004**, *54*, 217−224.
(41) Wei, L.; Fan, Y. J.; Ma, J. H.; Tao, L. H.; Wang, R. X.; Zhong, J. P.; Wang, H. *J. Power Sources* **2013**, *238*, 157−164.
(42) Dong, X. C.; Xu, H.; Wang, X. W.; Huang, Y. X.; Chan-Park, M. B.; Zhang, H.; Wang, L. H.; Huang, W.; Chen, P. *ACS Nano* **2012**, *6*, 3206−3213.
(43) Antolini, E.; Cardellini, F. *J. Alloys. Compd.* **2001**, *315*, 118−122.
(44) Pozio, A. D.; Francesco, M. D.; Cemmi, A.; Cardellini, F.; Giorgi, L. *J. Power Sources* **2002**, *105*, 13−19.
(45) DeYulia, G. J.; Cárcamo, J. M.; Bórquez-Ojeda, O.; Shelton, C. C.; Golde, D. W. *Proc. Natl. Acad. Sci. U. S. A.* **2005**, *102*, 5044−5049.
(46) Veal, E. A.; Day, A. M.; Morgan, B. A. *Mol. Cell* **2007**, *26*, 1−14.
(47) Snook, G. A.; Peng, C.; Fray, D. J.; Chen, G. Z. *Electrochem. Commun.* **2007**, *9*, 83−88.

(48) Hui, Y.; Bian, C.; Xia, S.; Tong, J.; Wang, J. *Anal. Chim. Acta* **2018**, *1022*, 1−19.
(49) Guo, W.; Wang, S.; Yu, X.; Qiu, J.; Li, J.; Tang, W.; Li, Z.; Mou, X.; Liu, H.; Wang, Z. *Nanoscale* **2016**, *8*, 1897−1904.
(50) Yajima, Y.; Yamada, M.; Utoh, R.; Seki, M. *ACS Biomater. Sci. Eng.* **2017**, *3*, 2144−2154.
(51) Block, M. L.; Zecca, L.; Hong, J. S. *Nat. Rev. Neurosci.* **2007**, *8*, 57−69.
(52) Marshall, S. A.; Mcclain, J. A.; Wooden, J. I.; Nixon, K. *Front. Neuroanat.* **2020**, *14*, 52.
(53) Masamune, A.; Watanabe, T.; Kikuta, K.; Satoh, K.; Shimosegawa, T. *Am. J. Physiol-Gastr. L.* **2008**, *294*, G99−G108.
(54) Germain, R. N.; Meier-Schellersheim, M.; Nita-Lazar, A.; Fraser, I. D. C. *Annu. Rev. Immunol.* **2011**, *29*, 527−585.
(55) Knutsdottir, H.; Condeelis, J. S.; Palsson, E. *Integr. Biol.* **2016**, *1*, 104−119.

https://doi.org/10.1021/acs.analchem.1c00621
Anal. Chem. 2021, 93, 7917−7924